American Mineralogist, Volume 76, pages 530–547, 1991

Hourglass inclusions: Theory and application to the Bishop Rhyolitic Tuff

A. T. Anderson, Jr.

The Department of the Geophysical Sciences, The University of Chicago, 5734 S. Ellis Avenue, Chicago, Illinois 60637, U.S.A.

Abstract

Hourglass inclusions are bodies of bubble-bearing glass in volcanic phenocrysts that extend to the crystal rim through a narrow neck. Compared to enclosed inclusions, hourglass inclusions are less devitrified, contain more gas, but contain less dissolved H_2O, CO_2, and Cl. Hourglass formation plausibly involves the unsuccessful capture of a gas bubble. Their evolution probably involves loss of some melt through the neck as a result of decompression in surrounding magma. The gas fraction attained within hourglass inclusions is governed by their size and shape as well as by both the amount and duration of external decompression. A quantitative model of rhyolitic hourglass emptying is developed and applied to Bishop Tuff hourglass inclusions. Those in plinian pumice suggest rapid ascent at 10 m/s consistent with theoretical eruption models. Hourglass inclusions from the Mono ash-flow lobe of the Bishop Tuff suggest (1) initial crystallization of quartz, formation of some enclosed and some hourglass inclusions at approximately 2400 bars; (2) magma decompression to approximately 1100 bars for at least a week (duration of eruption for the Bishop Tuff?) while hourglass inclusions further evolved and bubbles of gas attained a 50 μm diameter; (3) magma ascent from 1100 to approximately 700 bars at approximately 1 m/s, consistent with theory for ash-flow-producing (collapsing) eruption columns; (4) entrainment of some crystals that had decompressed to a pressure of 400 bars for several weeks; (5) thermal quenching of hourglass evolution as magmatic foam disrupted into fast-moving spray, erupted, and entrained cold air. Pressure at quenching is greater than predicted magma disruption pressures but possibly consistent with preservation of long vesicles. Uncertainties are large but can be reduced by future studies of postdepositional cooling, hourglass volatile compositions, temperature, and viscosity to obtain estimates of eruptive and preeruptive magma movement and crystallization rate.

Definition, occurrence, and significance

Hourglass inclusions are characterized by a narrow neck of glass connecting a larger body of glass in a crystal with its rim (Figs. 1 and 2). Reentrants differ from hourglass inclusions in that they have wide, open necks (Fig. 3).

In addition to the Bishop Tuff, hourglass inclusions occur in the upper Bandelier plinian quartz phenocrysts (Anderson, unpublished data), in the youngest Toba Tuff (Chesner, personal communication, 1990), and Paleozoic clay (Kozlowski, 1981).

Although various inclusions occur in various hosts, this work is about hourglass inclusions and enclosed inclusions of glass (including partially devitrified or crystallized glass) in phenocrysts of quartz. Consequently, inclusion as used here signifies a wholly enclosed glass inclusion in quartz. Hourglass means hourglass inclusion in quartz.

The significance of hourglass inclusions lies in their relation to the eruptive process. Volatiles in glass inclusions can be used to constrain or reveal crystallization pressures; these may be greater than the pressure of preeruptive magma storage. Pumice, on the other hand, is so decompressed that it is difficult to restore its preeruptive pressure because the pressures at which it rigidified and degassed are uncertain (Whitham and Sparks, 1986; Sparks and Brazier, 1982). Hourglass inclusions are intermediate: they decompress, but only partially, through a retarding constriction. Because hourglass inclusions are gas saturated, pressure within an hourglass inclusion can be inferred from its volatile composition, or from its gas content if its initial bulk volatile content can be ascertained (e.g., assumed equal to that in enclosed inclusions). Thus, hourglass inclusions trace magmatic decompression.

In the pages that follow, I first outline a quantitative model of melt loss through the necks of hourglass inclusions as a result of external decompression. Second, I review the geology and petrology of the Bishop Tuff and describe and compare its enclosed and hourglass inclusions. Third, I discuss, in the context of the Bishop Tuff, the problems of (1) diffusive boundary layers in melt, (2) contraction resulting from the β-α inversion of quartz, and (3) preferential rupture of gas-rich inclusions. Fourth, I use textures and compositions of enclosed and hourglass inclusions to suggest an origin for the Bishop hourglass

0003–004X/91/0304–0530$02.00

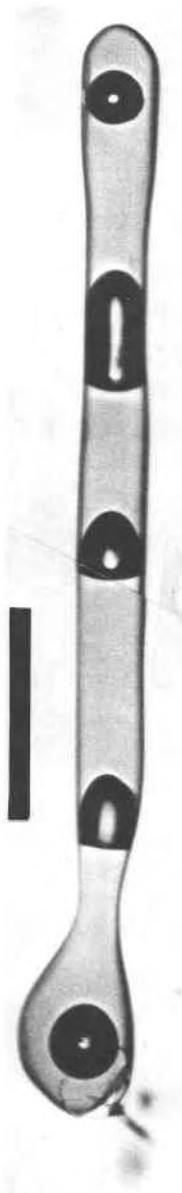

Fig. 1. Mono ash-flow hourglass LV81-18A-20. Scale bar is 250 μm long. The neck of the hourglass is at the bottom right. It points down out of the depth of focus and is approximately 100 μm long and 7 μm in diameter. When this photo was taken, the glass in the neck had been largely dissolved in HBF_4, a small portion of the glass in the hourglass near the neck was also dissolved; weak lines near the neck mark the boundary of the glass and refractive index liquid filling the acid-etched neck. The bubbles are subequally spaced and one bubble is more than twice as large as the others. Three of the five bubbles wet the wall of the quartz container. The three bubbles are asymmetrical such that the glass-bubble wall nearest the neck is less curved than the other. The asymmetry decreases in sequence away from the neck. Adjacent to the bubbles are narrow zones of less devitrified glass (this glass has strain birefringence probably caused by hydration from the high-pressure H_2O-rich gas initially present in the gas bubbles during post depositional cooling). The long dimension of the hourglass is parallel to **a**. The glass has been analyzed by electron microprobe and infrared (IR) spectroscopy at three spots: spot 1 between the first and second bubbles near the top end, spot 2 between the third and fourth bubbles, and spot 3 between bubbles four and five near the neck (see Table 2). Textural and compositional features combine to indicate that this hourglass was repressurized before eruptive quenching.

←

inclusions. Fifth, I apply the melt loss model to the Bishop Tuff hourglasses to estimate (1) the pressure at which rapid cooling stopped melt loss (plausibly near the pressure at which slow-moving magmatic foam disrupts into accelerated spray); (2) the duration of hourglass melt loss and decompression; and (3) some rates of ascent of the erupting magmas.

Quantitative model of hourglass emptying

I consider a fractional emptying process (Fig. 4) whereby the hourglass cavity is assumed to lose melt but not gas. As melt is lost, the remaining melt and gas decompress and equilibrate within the cavity. There results a relation between the pressure and volume fraction of gas in the hourglass. The fractional process differs only slightly from that for closed system decompression. With loss of melt, the total mass fraction of volatile material in the system increases with decompression rather than remaining constant. Consequently, the volume and mass fractions of gas increase more per increment of decompression in a fractionating hourglass than in a closed system.

In Appendix 1,[1] I derive and solve a differential equation that equates a decrease in the H_2O content of the inclusion with the amount of H_2O dissolved in the lost melt. The expression is similar to many fractionation equations, but the variables cannot be easily separated because there is a square root of pressure rule for the solubility of H_2O in the melt. The equation is a first order, linear differential equation and can be integrated using the standard procedure. The variables are (1) the initial pressure [or concentration of H_2O dissolved in the melt (glass)]; (2) the volume fraction of gas present at the initial pressure; (3) the final volume fraction of gas in the hourglass; and (4) the final pressure in the hourglass. The process is assumed to be isothermal, as a simplifying approximation. In practice, it is possible to infer the initial pressure from measurements on enclosed inclusions, and to measure in the hourglass both the proportion of gas and the concentration of H_2O dissolved in the melt. Consequently it is possible, in principle, to solve for the proportion of gas present before decompression began.

I next consider the case where CO_2 as well as H_2O is present. This sufficiently complicates the problem that a

[1] A copy of Appendix 1 may be ordered as Document AM-91-453 from the Business Office, Mineralogical Society of America, 1130 Seventeenth Street NW, Suite 330, Washington, DC 20036, U.S.A. Please remit $5.00 in advance for the microfiche.

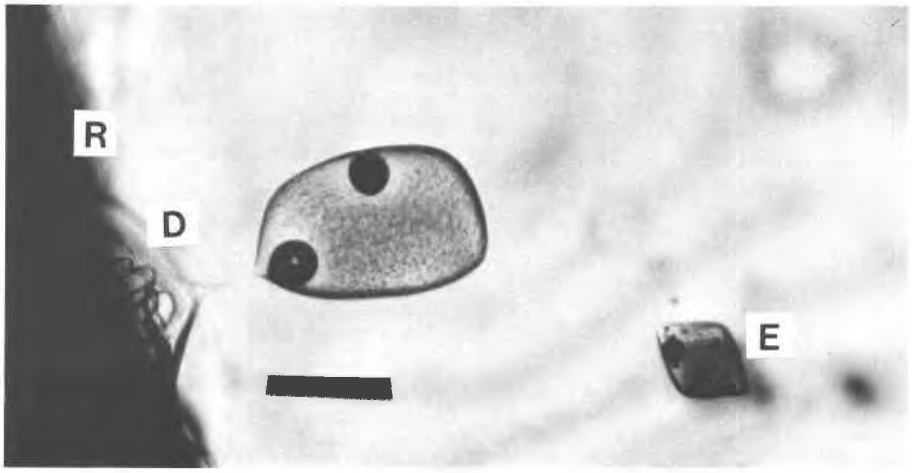

Fig. 2. A typical Mono hourglass showing subequal bubbles surrounded by finely devitrified brown glass. Note the near rim (R) position of the hourglass and its round shape compared with the enclosed inclusion (E). Where the barely visible neck connects with the rim of the quartz there is a depression or dimple (D) approximately 100 μm in diameter and 20 μm deep. The hourglass neck is roughly perpendicular to the faceted rim of the quartz phenocryst. The scale bar is 100 μm long.

numerical approach is needed. In addition, I take into account gas nonideality and species-dependent solubility relations. Gas fraction and pressure calculated for three relevant bulk compositions are in Figure 5. The important point is that the pressure within hourglasses can be inferred from the proportion of gas, if the initial bulk H_2O + CO_2 composition is known (e.g., from enclosed inclusions).

Dimensionless hourglass number, quenching pressure, and eruption duration

For a group of hourglasses with the same decompression history it is possible, in principle, to constrain both the duration and the external pressure of decompression from their gas volume fractions and geometries.

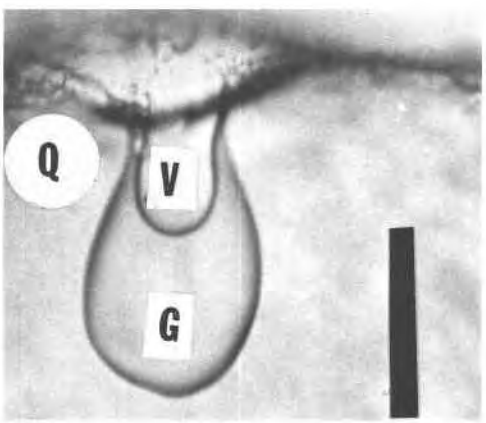

Fig. 3. Reentrant in rim of quartz (Q) largely filled with glass (G). The scale bar is 50 μm long. Refractive index liquid fills the void (V).

Imagine a magmatic history as follows (and see Fig. 4): stage 1, an hourglass forms in crystallizing magma at some pressure (P_0); stage 2, the magma rises (decompresses) instantly to a new lower pressure (P_1) and remains there for some duration of time (t); stage 3, the magma is instantly erupted and quenched. Qualitatively, if there are some hourglasses that would empty quickly because of short, wide-mouthed necks, then these will empty, during stage 2, nearly to the limit imposed by the new external pressure (P_1), from which the magma was quenched (stage 3). The gas fractions (g/V) in such hourglasses primarily

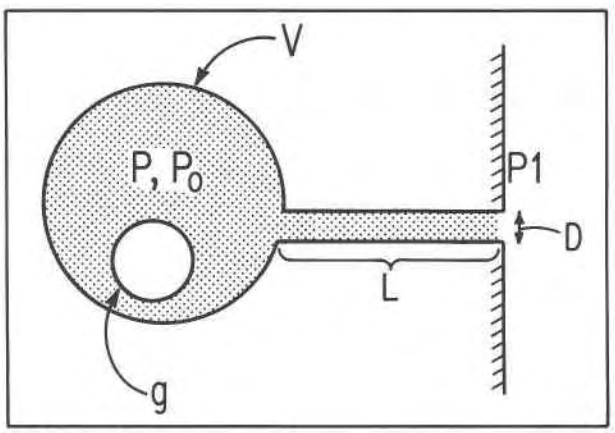

Fig. 4. Sketch illustrating the parts of an hourglass used in the mathematical derivation of the relations between gas fraction (g), the internal pressure (P and P_0), the external pressure P_1, the volume (V) of the hourglass, and the diameter (D) and length (L) of its neck. The dimensionless hourglass number [$HGN = V/(D^4/L)$] characterizes the sluggishness with which the volume fraction of gas will increase with time as melt escapes through the neck.

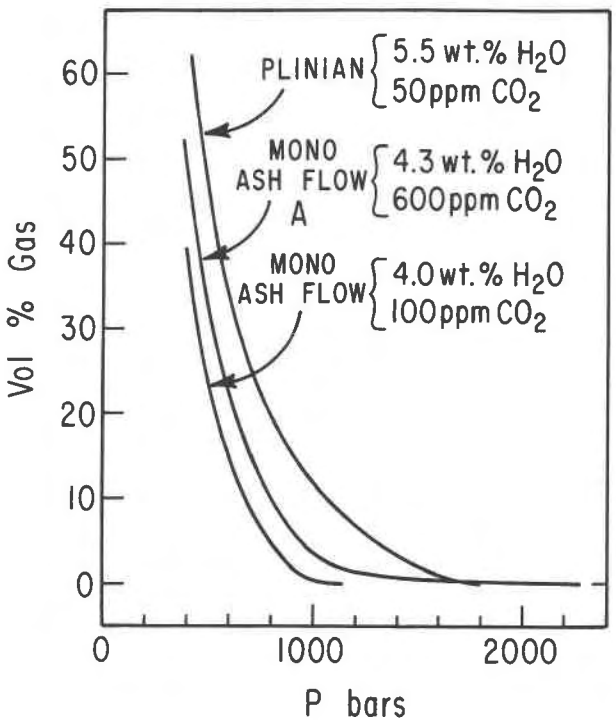

Fig. 5. Graph showing the relations between gas fraction and internal pressure in evolving rhyolitic hourglasses for three initial volatile compositions. The intercepts at 0% gas along the horizontal pressure axis give the respective gas saturation pressures. The curves for the plinian and Mono A conditions intersect at approximately 1700 bars, reflecting the important influence of a high CO_2 content (Mono A) in causing an initially rapid fall in pressure as gas is produced. The volatile compositions correspond to those used in modeling the Bishop hourglasses illustrated in Figure 6.

reflect the decreased external pressure (P_1). On the other hand, if there are some very sluggish hourglasses (with very narrow, long necks), then, upon eruptive quenching, these will retain an internal pressure (P) close to that of the initial pressure (P_0). Thus the gas fraction in the latter will reflect primarily the duration (t) of the decompressed stage 2. The exact solution for both time and pressure from the properties of a group of hourglasses with a common history depends on the quantitative details. These are presented in Appendix 1 and summarized below.

The rate at which melt will move out through a cylindrical neck by laminar flow is given by the Poiseuille equation (Eq. 19, Appendix 1). This leads to the formulation of a dimensionless quantity, here termed the hourglass number. It is the ratio of the volume of the hourglass to the fourth power of the diameter of the neck divided by the neck length. The hourglass number is a geometrical attribute of an hourglass, which expresses the combined effects of its total volume and the dimensions of its neck on the rate at which the proportion of gas in the hourglass will increase as a consequence of external decompression and consequent loss of melt through the neck. If an hourglass neck is narrow and long, then the absolute rate at which melt can extrude and gas volume increase will be small, but if the inclusion volume is also small, then, after a certain interval of time, the proportion of gas in the hourglass may be substantial. As defined, the emptying of an hourglass with a large hourglass number is relatively sluggish: its proportion of gas increases slowly compared to another hourglass with a smaller hourglass number.

The quantitative relations developed in Appendix 1 (Eq. 21) show that only two observable parameters [the volume fraction of gas ($G = g/V$) and the hourglass number [$HGN = V/(D^4/L)$] carry the principal information useful in evaluating the duration of time (t) and external pressure (P_1) common to a set of hourglasses. Some knowledge of temperature, melt composition, and initial volatile content is required so that the viscosity and initial pressure (P_0) can be established. For two hourglasses that formed during the same decompression history [($P_0 - P_1$) and t], as outlined above there is enough information (two equations with two unknowns) to calculate both P_1 and t. A useful graph (Fig. 6) shows the volume fraction of gas (G) vs. HGN with contours for various combinations of P_1 [strictly ($P_0 - P_1$)] and t.

The curves on Figure 6 were calculated by stepwise decreasing the pressure (P) within hourglasses and calculating, for successive pressure decrements, the corresponding increment of gas and the increment of time required for loss of sufficient melt through the neck to make room for the gas increment. The rate of loss of melt decreases with each pressure decrement because the melt viscosity increases as melt H_2O decreases and because the pressure gradient decreases. The accumulated total gas fraction and time calculated from the running sums yield the curves on Figure 6. The computational procedure is further described in Appendix 1.

The sigmoid shape of contour lines of equal time duration (isochrons) on Figure 6 reflects two qualitative boundary conditions: (1) for hourglass numbers larger than some limiting value, the accumulated fraction of gas is negligible; (2) for hourglass numbers smaller than some lower limit, the fraction of gas reaches the limiting value imposed by the external pressure. Thus there are two asymptotic limits to each isochron: (1) negligible gas fraction at very large hourglass numbers, and (2) equilibrium gas fractions at small hourglass numbers.

The transition between the asymptotic limits stretches over approximately 4 orders of magnitude of the hourglass number. The isochrons depend upon the initial concentrations of H_2O and CO_2 in the melt. Consequently, the isochrons on Figure 6 are peculiar to the Bishop Tuff and other magmas with similar H_2O and CO_2 concentrations. Separate computations are required for other conditions. Copies of the program (in Basic A) may be obtained on disk from the author. The program listing may be obtained from the author or from the journal (as part of Appendix 1).

An inverse problem arises if the decompression is not

instantaneous. Strictly, the emptying of any hourglass depends on the integral of the external pressure with respect to time. The above computations assume that the hourglasses are instantaneously decompressed to some new pressure at which partial emptying occurs before quenching. The extent to which an array of observations follows a single isochron for the instantaneous case is a measure of decompression rate. The instantaneous isochrons are useful as interpretive guides and should not be regarded as lines to which error-free data should conform.

The external pressure inferred for melt loss from a group of hourglasses is roughly the pressure at which emptying ceased. The particular eruptive process responsible for quenching the hourglass emptying would need to be rapid compared to the emptying rate of the hourglasses with the smallest hourglass numbers. Such Bishop hourglasses would attain observed gas fractions in minutes at crystallization temperature but would rigidify below 600 °C; rapid cooling plausibly begins when magmatic foam disperses into spray (magma fragmentation of Wilson et al., 1980). In view of the essential role of rapid cooling, it is appropriate that the pressure inferred for rigidification be termed the quenching pressure and be related to the pressure for magma disruption.

Background geology and petrology of the Bishop Tuff

The Bishop Tuff formed 0.73 Ma when approximately 600 km³ of rhyolitic magma erupted from the site of Long Valley caldera on the eastern margin of the Sierra Nevada in east central California (Gilbert, 1938; Sheridan, 1965; Bailey et al., 1976; Hildreth, 1977, 1979). It consists of a basal, sorted, and stratified plinian ash-fall deposit and a group of poorly sorted ash-flow tuff sheets termed lobes. The Bishop Tuff may be divided into two gradational parts on the basis of crystallization temperature and presence of pyroxene phenocrysts: (1) an early-erupted, pyroxene-free part consisting of the plinian ash-fall deposits and overlying ash-flow lobes with relatively low phenocryst crystallization temperatures, and (2) a later-erupted, pyroxene-bearing part consisting of higher temperature ash-flows (Hildreth, 1977, 1979). Phenocryst compositions vary approximately monotonically with Fe-Ti oxide equilibration temperature and stratigraphic position (Hildreth, 1977, 1979). This monotonic pattern together with the uniformity of phenocryst compositions within individual samples (individual pumice clasts or closely related materials) reveals that little or no mixing occurred before and during eruption. Evidently, neither crystal settling, nor convection, nor even eruptive turbulence mixed thermally varied parts of the magma. The important implication is that either there were separate bodies of magma or there was a single magma body that was stably stratified (nonconvecting before eruption and sequentially tapped during eruption) or the compositional zonation of the magma developed during the eruption.

Gas saturation in the Bishop magma is likely. Hildreth (1977, 1979) estimated that the Bishop plinian magma

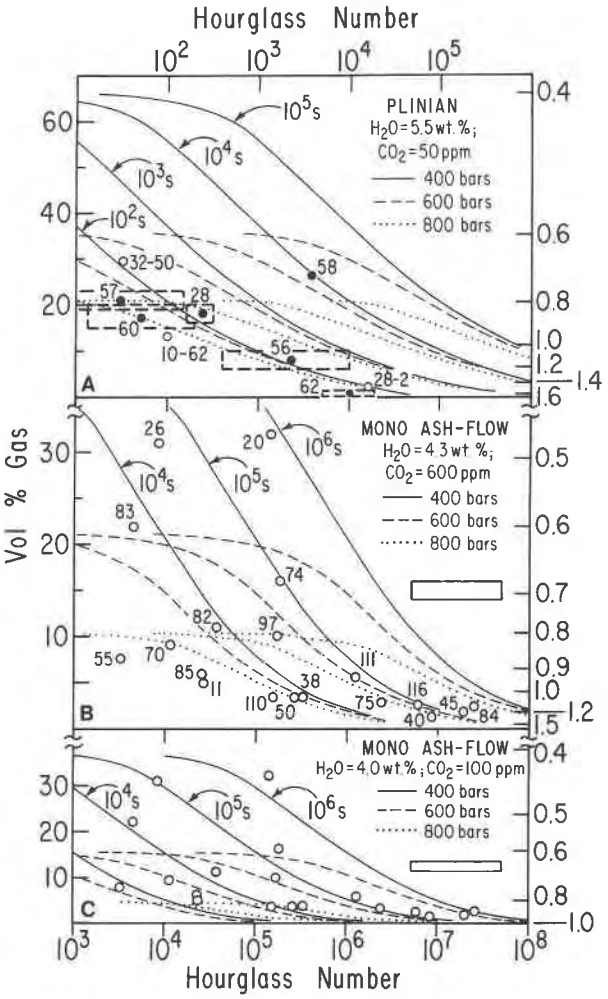

Fig. 6. Graphs of hourglass number and gas fraction contoured for various times and external pressures with parameters selected for the Bishop plinian magma (**A**) and the Mono ash-flow magma (**B**) and (**C**) as in Figure 5. The horizontal scales differ: the scale for **A** is shown at top, **B** and **C** at bottom. Each graph has three sets of curves (isochrons) corresponding to external pressures of 400, 600, and 800 bars as shown. Only the 400 bar isochrons have time value labels (e.g., 10^5 s) for clarity. As all equal-valued isochrons merge in the limit of low vol% gas, the values for the 600 and 800 bar isochrons are readily identified from those for 400 bars. The values ticked off along the right side of the graphs give the pressure in kilobars corresponding to the equilibrium vol% gas on the left (from Fig. 5). The size of the boxes provides a guide to the uncertainty in the hourglass number and the gas fraction. Individual boxes are given for some plinian hourglasses, as these vary depending on complexity of shape. The uncertainty in vol% gas is 10% to 20% relative, thus the absolute uncertainty (box height) diminishes downward toward the 0% gas value. The vertical scale is expanded in **B**. Three hourglasses are not plotted (see Table 1).

was close to saturation with respect to pure H_2O gas and that the higher temperature magma was not. Although Hildreth's estimations have large uncertainties, his interpretation is not inconsistent with saturation of even the

Mono lobe magma with a gas rich in CO_2 as inferred by Anderson et al. (1989a). Anderson et al. (1989b) argue that the pyroxene-free magma contained approximately 1–2 wt% of excess gas when inclusions formed in crystallizing quartz.

The rate of deposition of the Bishop Tuff appears to have varied because the ash flows have multiple zones of welding, compaction, and devitrification (Sheridan, 1967; Hildreth, 1977). However, the nature of the variations is argued. Snow and Yund (1988) have interpreted variations in the exsolution in sanidine phenocrysts from a thick ash flow to signify an eruptive-depositional interlude amounting to approximately 1 yr. Hildreth (1979) considered that the continuity of welding and negligible erosion suggests a single continuous eruption. Although some high-temperature material forms part of the early eruptive sequence south of the caldera, it is uncertain whether the high-temperature Mono ash-flow lobe north of the caldera formed at a significantly later time.

Samples

I have studied clasts of pumice from the plinian deposit and the high temperature, late-erupted Mono ash-flow lobe. There is notable textural variability between clasts of pumice from the same stratigraphic level. This study reports work on the following samples:

1. One 30-cm clast of long-vesicle, pyroxene-phyric pumice from the Mono ash flow: LV81-18A. The clast is from nonwelded, vitric ash-flow tuff within a few meters of underlying Sierran granite at the Aeolian Buttes (B-77 of Hildreth, 1977). The clast has a 2 cm thick buff rim around a white core.

Approximately 100 m north and 20 m downhill from the sampling locality, the Mono ash flow is densely welded and vitrophyric. Whether the difference in welding reflects differences in depositional temperature, cooling rate, or overburden pressure is uncertain.

2. Pumice clasts (LV81-32) from a proximal pumice-fall deposit at Sherwin summit on old U.S. highway 395 (locality B-2 of Hildreth, 1977). Tragically, the clasts were combined and treated as a single sample.

3. Two 3-cm clasts of pumice (B104-F, G) from a more distal pumice-fall location from Hildreth's B-104 sample (collected and donated by Hildreth).

Sample preparation

Crystals of quartz were extracted from clasts of pumice by gentle crushing and by using heavy liquids or H_2O to float off most of the glass. Glass was removed from the surfaces of some quartz crystals by solution in HBF_4. The crystals were immersed in 1.55 refractive index liquid for hours to days before handpicking to allow time for the liquid to penetrate cracks and vapor bubbles in cracked inclusions.

Primary gas bubbles and gas saturation

Primary gas bubbles in quartz would indicate that the magma from which the quartz and inclusions formed was saturated with gas. A primary gas bubble is one that is too large to have formed solely as a result of preferential shrinkage of melt and too isolated to have formed from necking down (Roedder, 1979). In the Bishop quartz, bubbles that comprise greater than approximately 2 vol% of uncracked, glassy inclusions are potentially primary.

Gas saturation means that gas is present. H_2O saturation means that a gas is present that is virtually pure H_2O. A magma can be gas saturated without being H_2O saturated. The proportion of gas could be large or small.

This work calculates solubilities and gas saturation pressures for rhyolite by using Silver et al. (1990) for H_2O and Blank et al. (1989) for CO_2.

Analytical methods

H_2O and CO_2 dissolved in one hourglass were determined by infrared (IR) spectroscopy following Newman et al. (1988). Some analyses were reported previously (Anderson et al., 1989a). Some hourglasses were analyzed by electron microprobe.

Determination of hourglass dimensions

The diameters of hourglass necks are critical for estimating durations of decompression because the time is inversely proportional to the fourth power of the diameter. Quartz samples were positioned in 1.55 index oil and the neck diameters were measured microscopically. Absolute uncertainties are approximately 0.5 to 2 μm. Some necks narrow toward the crystal rim and some are oval in cross section. Generally, I recorded and used the smallest neck diameter in the computations.

Neck lengths were measured similarly. A pythagorean correction was made if necessary.

Most hourglass volumes were estimated from two principal diameters measured in plan view. Some crystals were repositioned so that the hourglass and its neck could be viewed in another perspective.

Structures and textures of Bishop pumice, quartz, and inclusions

Introduction

Certain features of the pumice, quartz, and inclusions help evaluate whether hourglasses form and empty during special episodes of magma evolution, quartz growth, gas bubble nucleation, pre- or syneruptive decompression, or posteruptive cooling. I present evidence that some features (vesicle size and inclusion shape) that might be assumed to be of posteruptive origin are at least partly of preeruptive origin.

Pumice

The size, shape, and abundance of vesicles in Bishop pumice vary from clast to clast at the same stratigraphic level and within single clasts. Codeposited clasts had different histories of vesiculation.

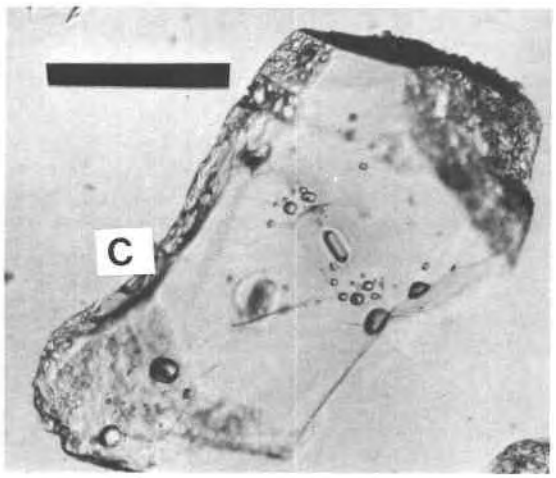

Fig. 7. A conchoidally fractured surface (C) on a quartz phenocryst from the Mono ash flow. The conchoidally fractured surface is near the 200-μm scale bar and subperpendicular to the plane of the picture. Finely vesicular glass covers the entire fracture but is missing from most of the fractured surface parallel to the plane of focus. The glass-coated fracture formed first in a melt-rich environment, and the uncoated fracture formed later in a melt-poor (gas-rich) environment.

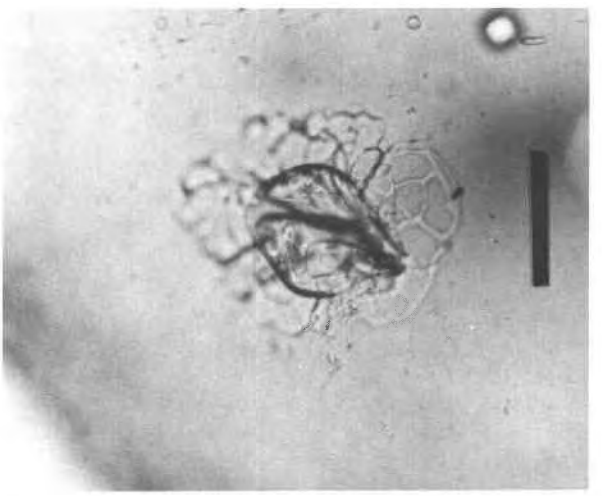

Fig. 8. A burst inclusion spread out over part of a fracture in a Mono quartz phenocryst. The incomplete coating of natural fractures with glass indicates that some fracturing occurred in a gas-rich environment probably after the ambient external melt lost the ability to flow. Scale bar is 50 μm.

Quartz

Phenocrysts of quartz are 1–8 mm diameter subhedral bipyramids. The crystal surfaces include flat faces, round parts, and conchoidal fractures. All flat faces and some conchoidal surfaces (Fig. 7) are coated with vesicular glass. Fractures are both preeruptive (glass coated) and posteruptive (glass free). Many conchoidal surfaces are partly free of glass and intersect one or more cavities (Fig. 8), formerly inclusions of melt which burst. Such surfaces and burst inclusions plausibly formed in a gas-rich (possibly posteruptive) environment. Most of the quartz mass consists of mostly faceted fragments comprising more than approximately half of the unfractured initial crystal. About one in ten grains larger than 0.5 mm are euhedra. Compound grains of quartz containing two or more crystals are virtually absent. The quartz fragments evidently reflect natural and laboratory fragmentation of free-swimming individual crystals and no dislodgement of crystals from intergrown aggregates and magma walls.

Glass coatings are thin and finely vesicular on most plinian quartz and on all studied ash-flow quartz. Some plinian quartz has thick coatings of glass with thick-walled vesicles (Fig. 9). Because crystals with thick and thin glass coatings occur in the same clast (e.g., B104-F), it seems likely that variable outgassing occurred prior to pumice clast formation and extrusion.

Inclusions, hourglasses, and reentrants

There are significant variations in the devitrification, size, shape, abundance, and distribution of, and bubbles within, inclusions, hourglasses, and reentrants. Some variations occur within individual crystals and likely reflect preeruptive events. Others occur within and between pumice clasts and rock type and may reflect processes that took place after deposition, as well as before extrusion. The aim of this section is to describe and evaluate certain features that relate to the formation and evolution of hourglasses before, during, and after eruption and deposition.

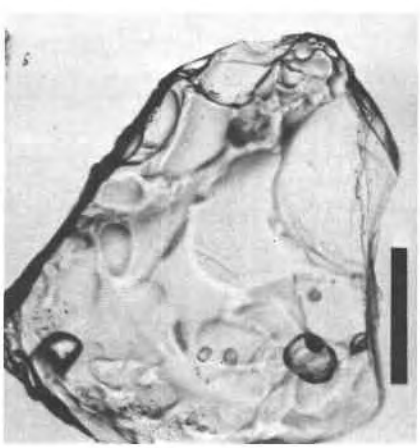

Fig. 9. A thick coating of glass on a quartz phenocryst from plinian clast B104-F. The glass coating lacks tiny vesicles such as those seen in Figure 7, but has portions of large bubbles. Glass adhering to other crystals of quartz from the same clast of pumice is finely vesicular like that shown in Figure 7. The various sizes of bubble segments comprising attached glass on different crystals in the same clast of pumice suggests variable outgassing of melt prior to formation of pumice clasts. The scale bar is 200 μm long.

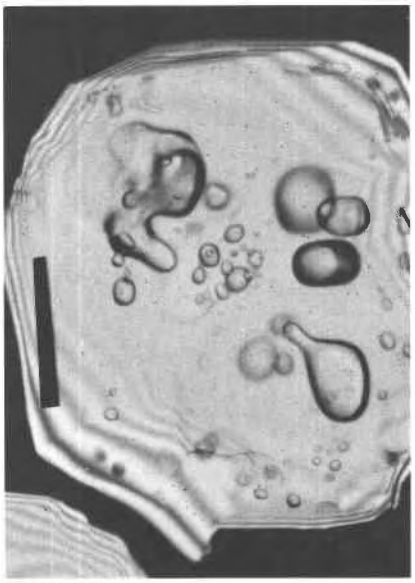

Fig. 10. A plinian quartz phenocryst with large irregular inclusions of glass. Numerous small inclusions occur throughout the quartz and most are smooth and equidimensional, but some near the rim are elongate. The scale bar is 400 μm long.

Plinian inclusions, reentrants, and hourglasses are colorless and not devitrified (Figs. 10–11). Mono ash-flow inclusions from sample LV81-18A are devitrified (Fig. 12), and the most finely devitrified (speckled) ones occur near crystal rims (Fig. 13). The most coarsely devitrified Mono inclusions are smaller than approximately 20 μm, but many tiny inclusions are poor in devitrification products (Fig. 14). Mono reentrants are vitric (Fig. 3), as is the glass that coats quartz crystals. Mono hourglasses range from vitric (clear to brown and generally gas rich) to very finely devitrified (speckled and generally gas poor).

Devitrification is promoted by slow cooling and high H_2O in melt or glass; devitrification of Mono inclusions reflects slow cooling because their 4.0% H_2O compared to 5.5% in plinian inclusions (Anderson et al., 1989a; Skirius et al., 1990) would inhibit devitrification (for example degassed glass in reentrants and attached to crystal surfaces is not devitrified). Some Mono hourglasses and reentrants are vitric because of low H_2O content compared to inclusions (the reentrants cooled at the same rate as the inclusions). Extension of this reasoning suggests that fine devitrification of near-rim Mono inclusions reflects low H_2O melt of preeruptive origin. Increased coarsening of hourglass devitrification (colorless to brown to speckled) with decreasing gas fraction is consistent with greater melt H_2O in gas-poor (less outgassed) hourglasses.

Fig. 11. A plinian hourglass with a large range of bubble sizes. The hourglass neck is poorly visible because it was largely dissolved with HBF_4 and replaced with refractive index oil. The dark edge of the photo is 400 μm long.

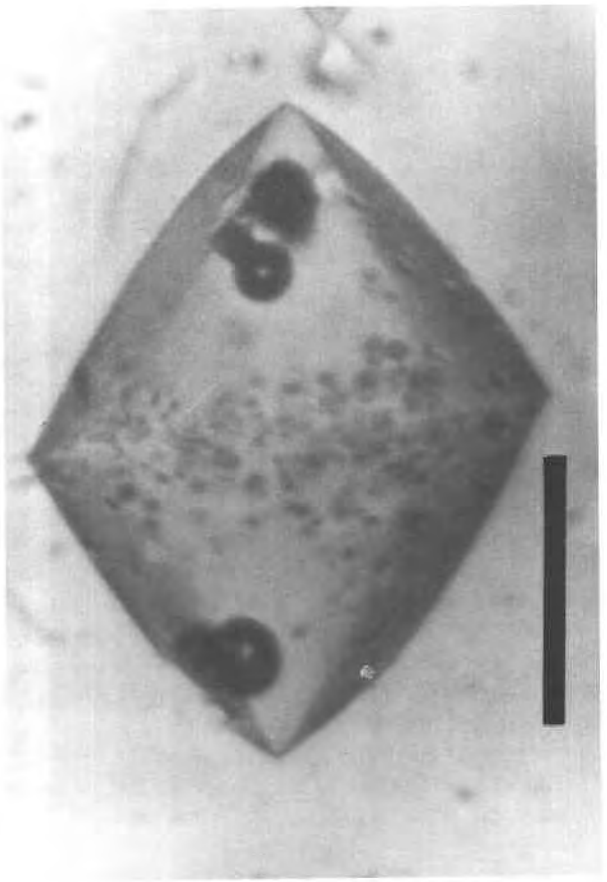

Fig. 12. An enclosed inclusion in Mono quartz showing devitrification speckles, sharp corners and edges, gas bubbles, and daughter crystals attached to the bubbles. The scale bar is 100 μm long.

Most plinian inclusions are smooth and spherical, but some that are smaller than 50 μm are partly faceted. Plinian hourglasses and reentrants are also smooth. Mono inclusions from sample 18A are angular (faceted—Fig. 12) to smooth (Fig. 15). Although some faceted inclusions occur near crystal rims, in crystals that contain both angular and smooth inclusions, the smooth inclusions are nearest the rim.

The faceted shapes of Mono inclusions are preeruptive in origin because both round and faceted inclusions are from the same clast and are similarly devitrified indicating similar compositions as well as posteruptive cooling.

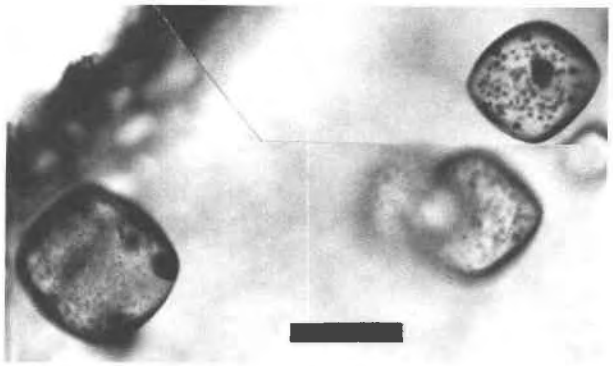

Fig. 13. Variably devitrified inclusions in a Mono quartz. The larger inclusion near the glass-coated rim of the quartz is more finely devitrified. The photo is a mosaic because the two inclusions are different focusing depth positions. A 100-μm scale bar.

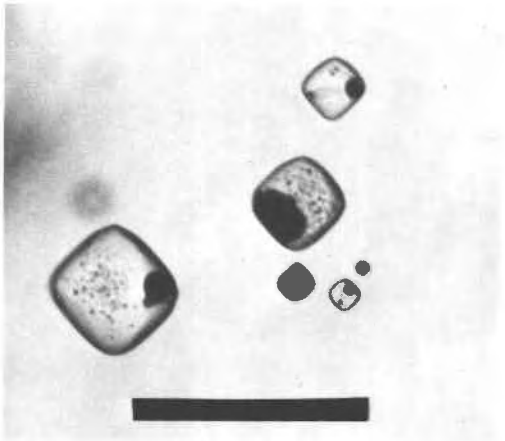

Fig. 14. Variably devitrified, bubble-bearing Mono inclusions. The smaller inclusions are most extensively devitrified. Scale bar is 100 μm long.

Both kinds should, therefore, have annealed similarly during posteruptive cooling; their differences must be preeruptive in origin. Beddoe-Stephens et al. (1983) suggested that faceting of inclusions reflects time-dependent annealing. Although preferential faceting of small plinian inclusions suggests more rapid annealing due to smaller distances for solution and redeposition, the spatial arrangement of faceted and round inclusions in Mono quartz suggests a dominant effect of time. Preeruptive evolution of hourglasses might be associated with preeruptive annealing of Mono inclusions.

Bubbles are rare in plinian inclusions but almost everpresent in inclusions from Mono ash-flow sample 18A. Most inclusion and hourglass bubbles are smooth and spherical, but some plinian hourglass bubbles are long with sharp ends. Bubbles are smaller than approximately 15 μm in inclusions and generally increase in size with inclusion size. Hourglasses have conspicuously larger bubbles up to approximately 100 μm. Single bubbles in Mono inclusions increase in size up to approximately 15 μm with increasing inclusion size; larger inclusions (approximately 100–150 μm) that might contain larger single bubbles, instead contain multiple bubbles that commonly are evenly spaced; many Mono inclusions larger than approximately 150 μm have no bubble. All small Mono inclusions have a bubble. Most bubble-bearing inclusions have only one bubble, but hourglasses commonly have several. Reentrants generally lack bubbles. Multiple bubbles in plinian hourglasses vary in size by approximately a factor of five, but those in Mono inclusions and hourglasses are similar in size and are commonly subequally spaced. Bubbles make up less than approximately 4 vol% of inclusion volume, except for Mono inclusions that are smaller than approximately 20 μm. Bubbles make up 2–32 vol% of most hourglasses (Figs. 1, 2, 11, and 16 and Table 1).

When most bubbles formed, the melt was hot enough to flow and form smooth spherical bubbles, but some bubbles were quenched into long shapes that formed as melt flowed outward through plinian hourglass necks. The small bubble size, small gas fraction, and increase in bubble size with inclusion size indicates that inclusion bubbles formed after inclusions were isolated (Roedder, 1979), but possibly before eruption.

Some bubbles probably formed before eruption: two analyzed bubble-bearing plinian inclusions (B104-F-6 and -21) have greater CO_2 dissolved in the glass than bubble-

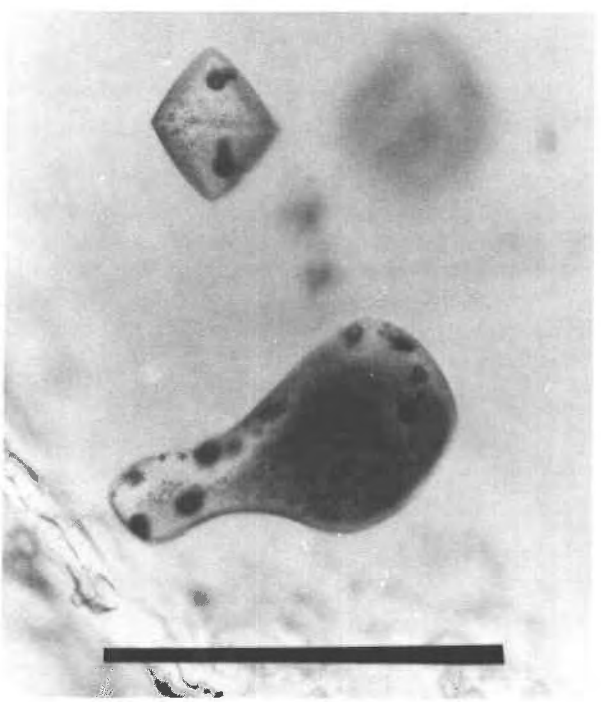

Fig. 15. Round and faceted inclusions in a Mono quartz. The larger, rounder inclusion extends to a position closer to the glass-coated rim of the quartz. The scale bar is 200 μm long.

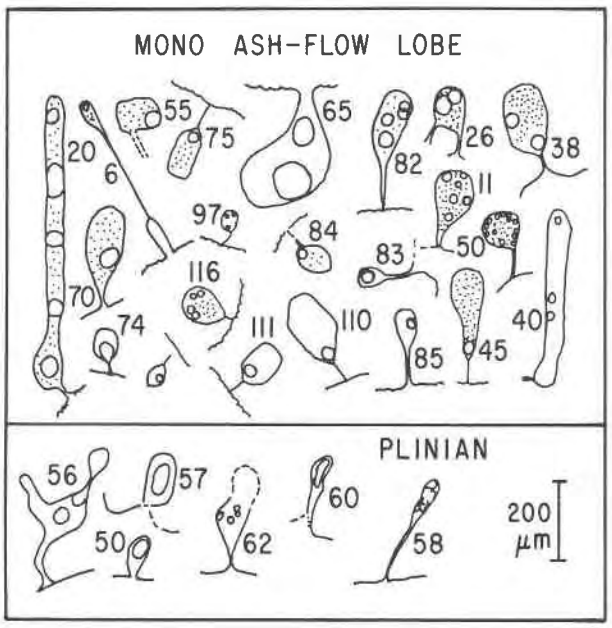

Fig. 16. Line drawings of hourglasses. Individual inclusions are numbered, corresponding with Table 1. Stippling indicates brown devitrification of glass. Bubbles are unstippled.

TABLE 1. Textural data on hourglass inclusions

No.	*V*	*D*	*L*	*HGN*	Gas	Bubs	Notes
Pinian hourglasses							
F-1	0.6	25	30	0.0046	80	many	j
F-28	1.9	32	130	0.024	18	6	
F-28-2	0.39	7.5	120	1.48	2	2	c
F-56	1.3	19	170	0.21	8	2	h
F-57	1.07	20	50	0.03	21	1	d
F-58	0.15	10	250	0.37	27	9	d, g
F-60	0.16	20	50	0.005	17	3	
F-62	1.1	8.5	50	1.0	0.8	4	a, h
32-50	0.51	30	50	0.0031	30	1	a
G10-62	0.5	30	150	0.01	13	7	g
G10-30	0.68	20	50	0.02	80	15	g, k
Mono ash-flow lobe hourglasses							
11	1.2	7	50	2.5	5	6	b, d
20	3.4	7	100	14.2	32	5	a, b
23	2.0	29	20	0.0057	60	6	b, c, i, ?k
26	0.68	10	120	0.82	31	2	b, d, e
38	0.78	3	30	29	4	2	a, b
40	1.97	2	70	860	1.5	3	c
45	1.47	1.5	68	1970	2	1	b, f
50	0.84	4.5	110	22.5	4	13	b, g
55	0.64	14	211	0.35	7.5	1	b, g
65	15.9	37	38	0.0322	10	2	a, i
70	2.8	12	80	1.1	8.7	1	b, g, h
74	0.38	3	39	18.3	16	1	d, f
75	0.42	1.9	80	237	2.8	1	c, b
82	1.14	7.5	99	3.7	11	4	n, h
83	0.14	6	40	0.43	22	1	a, g
84	0.42	<1.0	?60	2550	2.5	1	b, c, f
85	0.19	5	82	2.5	5.8	1	b, c
97	0.08	2	37	18	10	3	d
110	0.92	3.7	31	15.3	3.2	1	b, c
111	0.33	1.9	37	103	5.5	1	b, c
116	0.49	1	12	590	2.6	4	b, a

Note: No. = inclusion number [nos. F-1 to F-62 from B104 (Hildreth, 1977) pumice clast F; nos. 11–74 from Mono ash-flow pumice block LV81-18A; no. 32-50 from plinian pumice LV81-32; nos. G-10-30 and G-10-62 from B-104 pumice clast G]; V = volume of hourglass inclusion in units of 10^{-6} cm^3; D = diameter of hourglass neck in μm (10^{-6} m); L = length of neck in μm; HGN = dimensionless hourglass number = $[V/(D^4/L)] \times 10^{-4}$; Gas = volume percent of gas in the hourglass; Bubs = number of separate bubbles of gas in the hourglass; a = round shape; b = brown color; c = partly faceted shape; d = subround shape; e = two necks; f = bubble located near neck—gas lost from hourglass (?); g = neck terminates at a fracture; h = irregular neck; i = off scale on Figure 6 (not plotted); j = gas-filled neck (not plotted); k = surface glass-free (not plotted).

free inclusions (Anderson et al., 1989a). If the bubbles formed from melts similar to those typified by the bubble-free inclusions, then the CO_2 would preferentially enter the bubble and deplete rather than enrich the glass in CO_2. More CO_2 in bubble-bearing inclusions suggests formation at relatively high temperature and pressure: (1) cooling from a high entrapment temperature could cause crystallization of host quartz, preferential contraction of melt, and bubble formation; (2) a higher pressure of entrapment (associated with a high temperature) allows more CO_2 to dissolve in the melt.

The persistence of bubbles in the smallest Mono inclusions suggests that, contrary to the usual case (as for plinian bubbles) in which small inclusions are bubble-free (Roedder, 1979), there was, in the case of the Mono inclusions, plenty of time to nucleate and grow bubbles. Likewise, the similar sizes of multiple bubbles suggest surface energy (textural) equilibration typical of annealing. The puzzling absence of bubbles in the largest Mono inclusions may reflect mechanical collapse of quartz around the biggest (weakest) inclusions as melt cooled and contracted. This would only be likely at preeruptive pressures.

The large bubble size and gas content of hourglasses (as compared to inclusions) suggests decompression, loss of melt through their necks, and compensating bubble growth, as modeled above. Some gas volume in hourglasses may be primary, and some volume probably is the result of shrinkage during cooling.

The amount of gas in Mono inclusions provides a guide to the amount of gas in hourglasses that may be of shrinkage origin. For the Mono samples, the vol% of gas varies inversely with inclusion diameter (relations are unsystematic for plinian bubbles). Inclusions (including some with multiple bubbles) in ten Mono crystals roughly fit an inverse relation: $G = [2 \times G_0 \times d_0/(d + d_0)] - G_0$, where G_0 is the extrapolated percent of gas in an infinitesimally small inclusion ($d = 0$), and d_0 is the linear dimension (e.g., equivalent diameter) of the smallest inclusion that is bubble free. For the Mono samples, the value of d_0 is between 150 and 250 μm and extrapolated G_0 is around 4 vol% regardless of inclusion shape. Inclusions that are comparable in size to most hourglasses (larger than approximately 100 μm equivalent diameter) have less than approximately 0.5 vol% gas.

The numerous bubbles in plinian hourglasses and their greater range in size suggest continued nucleation caused by relatively rapid decompression. Low numbers of bubbles in Mono hourglasses, by comparison, suggest little or no bubble nucleation during decompression. If bubbles

nucleated during hourglass decompression, it is predicted that hourglasses with small hourglass numbers would nucleate and grow more bubbles owing to more rapid decompression. The evidence is equivocal on this point, but the lack of bubbles in most reentrants suggests that few bubbles nucleated during eruptive decompression. Although some postdepositional bubble modification seems probable, the small numbers and uniform sizes and spacings of Mono hourglass bubbles suggest nucleation before eruptive decompression.

Glass inclusions occur in most crystals of plinian and Mono quartz and are sprinkled from core to rim. Zones of inclusions are rare. Broad distribution of inclusions indicates that inclusions of melt were trapped in quartz phenocrysts at many stages. Rare zones of inclusions suggest that episodes of preferential formation were few.

Although most reentrants are free of bubbles, some, in contrast with hourglasses, have a gas tube that extends through the neck. Such reentrants could alternatively be considered to be gas-rich hourglasses. Because a gas tube raises questions about how melt and gas escaped, I did not consider such objects to be hourglasses.

Features of hourglasses are documented in Table 1 and displayed in Figures 1, 2, 11, and 16. Mono ash-flow sample 18A yielded 20 hourglasses out of a population of thousands of quartz crystals. In plinian samples, hourglasses seem less common, but may be more difficult to discern. Most hourglasses occur within approximately 300 μm of the rim of the crystal (most necks are shorter than 100 μm) and are slightly elongate in the direction perpendicular to the rim. The long dimensions of a few hourglasses are parallel to a [1000] direction. Such long inclusions commonly lie near and parallel to a poorly developed $(10\bar{1}0)$ face. Mono hourglasses are round with rare small facets, like large, near-rim enclosed inclusions. Hourglasses with large necks are gradational with reentrants, which also are round and largely unfaceted.

Because of their near-rim position, it is likely that Mono hourglasses formed later than most angular (faceted) enclosed inclusions. Mono hourglasses and near-rim, round inclusions may have formed together in response to a system-wide event.

That the necks of most hourglasses are growth-related is suggested by their orientation nearly perpendicular to a crystal face. A few terminate at conchoidal fractures with an oblique angle. Two hourglasses have two, roughly coplanar necks. The necks of the latter might have evolved from cracks.

The necks of all but a few hourglasses studied terminate on quartz surfaces that are completely coated with glass. Even the conchoidal fractures that terminate hourglasses (LV81-18A-50, LV81-18A-70, and B104-F-58) are completely coated with glass. Hourglasses that vented into a region that was hot enough and rich enough in melt so that melt could wet newly formed fractures, probably lost melt primarily before full vesiculation and extrusion. Rare, plinian hourglasses have a blob of vesicular glass adhering to the surface of the crystal at the end of the neck. Only hourglasses with glass-filled necks that terminate on glass-coated surfaces are plotted (Fig. 6) and interpreted.

Hourglass inclusion LV81-18A-20 (Fig. 1) is uniquely significant because of the large size, abundance, and peculiar shape of its bubbles. One of the five, almost equally spaced bubbles is at least twice as big as the next largest. Three of the bubbles wet the quartz walls and are asymmetrical with their most strongly curved sides away from the neck. Within each bubble there is a single cluster of radiating needle or blade-shaped birefringent crystals each up to approximately 20 μm long. The longest crystals and the biggest cluster of crystals are in the biggest bubble. Around each bubble there is a 20–40 μm wide region of glass that has strain birefringence and is less devitrified (lighter tan in color). The hourglass has been analyzed by microprobe for major elements and spectroscopically for H_2O and CO_2 near each end (Fig. 1). The results are listed in Table 2 and discussed further below.

The textural features of hourglass 20 are interpreted as follows: the bubble shapes (more highly curved away from the neck) are taken as evidence of late flow of melt into the hourglass. The largest bubble probably was the first bubble to form; possibly it was present in the hourglass when decompression began. The equal spacing of the bubbles probably reflects the effect of diffusion (mainly of H_2O) to increase the level of supersaturation with distance from bubbles. H_2O concentration and supersaturation and bubble nucleation rate would increase with distance from preexisting growing bubbles. New bubbles would preferentially nucleate near the point of maximum supersaturation midway between preexisting bubbles. The crystals on the bubble walls probably formed by reaction between bubble gas and melt or glass on the wall.

Chemical composition

Inclusions and hourglasses are high-silica rhyolite in both plinian and Mono lobe quartz. Although nonvolatile major, minor, and trace elements are similar in plinian and Mono inclusions (Anderson et al., 1989a; Lu et al., 1990; Lu, unpublished data), Mono inclusions are richer in K_2O and more variable in trace element composition. The work of Skirius (Skirius, 1989; Anderson et al., 1989a; Skirius et al., 1990; Skirius, unpublished data) reveals that in terms of dissolved volatiles, there are two groups of Mono inclusions: a high CO_2 group with CO_2 concentrations between 480 and 600 ppm and a low CO_2 group with CO_2 between 300 and approximately 50 ppm. The H_2O concentrations are similar for both groups (3.7–4.5 wt%). Low CO_2 inclusions are most abundant and occur in five of five clasts; rare high CO_2 inclusions are known in only two of the same five clasts. Angular and round inclusions are present in both groups. Plinian inclusions have more H_2O but CO_2 similar to the low CO_2 Mono inclusions. H_2O, CO_2, and Cl contents are lower in analyzed Mono lobe hourglasses than in inclusions (Anderson et al., 1989a; Skirius et al., 1990; Table 1). Hourglass LV81-18A-20 and two other Mono hourglasses have K_2O typical of plinian inclusions. Although the compositions

TABLE 2. Chemical compositions of hourglass and other glass inclusions

Sample	20-1	20-2	20-3	1	5	9	11-1	15	M	P
SiO_2	77.3	76.2	77.2	77.0	75.5	76.8	76.5	78.0	77.2	77.6
Al_2O_3	12.4	13.2	12.4	12.7	13.3	12.6	12.9	11.8	12.9	13.3
FeO	0.68	0.73	0.60	0.68	0.76	0.72	0.55	0.62	0.6	0.6
CaO	0.41	0.55	0.50	0.4	0.4	0.5	0.4	0.4	0.4	0.3
Na_2O	4.85	4.94	4.81	4.6	3.5	3.5	3.7	3.5	3.7	3.9
K_2O	4.37	4.45	4.53	4.8	6.1	5.8	5.9	5.9	5.9	4.6
Sum	95.8	95.9	96.0	95.9	93.6	96.7	96.2	94.5	94.3	92.5
H_2O	2.1*	nd	2.6*	2.2	4.6	4.5	5.0	3.6		
CO_2 (ppm)	21*	nd	25*	<50	360	255	280	145		
Cl	0.00	0.05	0.02	0.02	0.04	0.07	0.08	0.06	0.07	0.08

Note: All numbered columns are individual glasses from Mono ash-flow pumice block LV81-18A. Column M = average Mono enclosed inclusion glass (Anderson et al., 1989a, Table 1, col. 3); column P = average plinian enclosed inclusion glass (Anderson et al., 1989a, Table 1, col. 2); numbers 20-1, 20-2, 20-3 are separate analyzed spots on inclusion LV81-18A-20 (see Fig. 1), spot 1 at far end, spot 3 near the neck, spot 2 intermediate. Numbers 9 and 15 were homogenized by heating before analysis. Numbers 20 and 1 are hourglass inclusions, the others, including the averages, refer to enclosed inclusions.

* Average of two determinations. Major elements determined by electron microprobe using energy dispersive procedures and matrix corrections as programmed for the Chicago microprobe by Ian Steele, except for FeO and Cl which are based on crystal focusing spectrometers and aegerite and scapolite standards. Major element oxides are normalized to 100% (except for minor rounding errors) based on the original microprobe sum that is given in the sum row. H_2O and CO_2 determined by IR spectroscopy by C. Skirius at Chicago and Caltech using Nicolet 60SX instrumentation as developed by Stolper and Newman and explained in Anderson et al. (1989a).

of plinian and Mono inclusions are more similar to each other than are the respective bulk rocks, significant differences remain and indicate that the inclusions formed from distinct magmas. These facts reinforce the petrographic individuality documented by Hildreth (1977, 1979) for separate parts of the Bishop Tuff and magma: separate quartz crystals formed in separate environments and did not mix, except perhaps at a late stage when some hourglasses formed.

Melt inclusions and crystal growth

A concern is that melt inclusions will differ in composition from the ambient melt as a result of boundary layer processes (Watson et al., 1982). Except for one-component systems, a finite chemical potential gradient must surround any actively growing crystal; if there were no gradient, ingredients would not diffuse toward the crystal and growth would stop. This is so whether chemical diffusion is rate limiting or not. The extent of enrichment (or depletion) is limited by the need to continue growth. Growth of quartz, for example, requires that the melt next to the quartz has a lesser concentration of SiO_2 than that farther away. If the melt SiO_2 concentration next to quartz falls below the equilibrium value, growth of quartz may stop. Possibly quartz would continue to grow metastably from a melt with 70 wt% SiO_2 (10% depleted); such a melt might be in metastable equilibrium with quartz, but would be supersaturated with respect to sanidine, etc. The range in Al_2O_3 in inclusions and hourglasses is approximately 15% (from 11.8 to 13.6 wt%, Table 2) including analytical error (4%) and variation due to differentiation. Inverse correlations between compatible Mg, La, and incompatible U indicate that boundary layer rejection of trace elements from quartz is overshadowed by the expected effects of crystallization differentiation of the polymineralic modal phenocryst assemblage (Lu et al., 1989, unpublished data). Although analytically nondetectable boundary layer effects may influence nucleation (Bacon, 1989), boundary layer processes cannot have affected Bishop inclusion compositions except at levels less than approximately 10% relative.

Gas bubble volumes and the β-α inversion

Quantitative interpretations of hourglasses depend on gas bubble volumes. At approximately 575 °C (depending on pressure), cooling quartz crystals undergo a sudden 1% volumetric contraction due to the inversion from β to α quartz (Ghiorso et al., 1979). The vol% of gas in an hourglass or other inclusion might have been as much as 1% more (e.g., 1.1% rather than 0.1%) before the β-α inversion of the quartz host.

Causes of a lack of primary gas bubbles

Although the absence of large gas bubbles in large inclusions is suggestive of gas-free magma, Donaldson and Henderson (1988) reveal that bubbles will migrate away from growing quartz, and Tait and Jaupart (1990) imply that bubble-bearing inclusions would preferentially rupture upon eruptive decompression. Donaldson and Henderson (1988) placed quartz crystals in superheated, gas-saturated melt and showed that gas bubbles erode reentrants into dissolving quartz phenocrysts. The erosive drilling of bubble and melt into the quartz occurs because melt is swept around the surface of the bubble and brought toward the dissolving quartz in response to a gradient in surface tension. The gradient in surface tension arises because of the gradient in SiO_2 in the melt next to dissolving quartz. The transported melt accelerates the solution of the quartz because, coming from the side of the bubble farthest from quartz, it is more undersaturated with respect to quartz. If the quartz is crystallizing rather than dissolving, bubbles would migrate away from, rather than toward, the growing quartz surface. Because crystallization is required if a bubble is to become

trapped in quartz, bubbles must eventually tend to move away from the quartz. This is a plausible explanation for the absence of primary bubbles of gas in inclusions in quartz.

With isothermal decompression, inclusions larger than approximately ⅓ of the crystal are expected to rupture (Tait and Jaupart, 1990). Decompression is unlikely to be isothermal, and a few degrees of cooling per kilobar suffice to compensate for the elastic decompression effect. The survival of many inclusions up to 300 μm in size suggests that cooling during decompression has been sufficient to overcome the isothermal decompression effect. The survival of large inclusions with large bubbles is, however, problematical, because such inclusions would maintain high internal pressures owing to the expansivity of the gas. It is possible, therefore, that virtually all large bubble-bearing inclusions ruptured. Universal decrepitation of bubble-bearing large inclusions implies that all bubbles in surviving, large, uncracked inclusions formed as a result of posteruptive preferential contraction of melt. This is problematical for the two plinian inclusions mentioned above that are rich in CO_2 and contain bubbles, and this is impossible for the hourglasses. The near absence of large (possibly primary) gas bubbles in inclusions is poorly explained by preferential rupture.

The initial gas content of hourglass inclusions

The observed gas and dissolved volatile contents of an hourglass can be used to infer whether the hourglass contained a significant amount of gas before decompression. As an example, consider the plinian-like, Mono lobe hourglass LV81-18A-20 (Tables 1 and 2). The bulk CO_2 in the gas + melt hourglass (approximately 3000 ppm assuming equilibrium between melt and gas at the estimated gas-saturation pressure of 360 bars) is much greater than that of bubble-free CO_2-rich plinian inclusions (approximately 250 ppm CO_2, Skirius, unpublished data, 1989). The excess CO_2 points to the initial presence in the hourglass of 2750 ppm of gaseous CO_2 (approximately 2.5 vol% of CO_2-rich gas at 1400 bars).

The amount of gas estimated above is comparable with the observed difference in volumes of the two largest bubbles (approximately 5 vol% of the entire hourglass). Probably, this hourglass contained a primary CO_2-rich gas bubble approximately 50 μm in diameter at approximately 1400 bars.

Origin of hourglass inclusions

The hourglasses either contained primary gas bubbles or developed gas bubbles in the early stages of entrapment. The following reasoning shows that a bubble helps an hourglass remain open. A 200-μm inclusion will thermally equilibrate with its surroundings in less than 0.01 s, and a 2-mm quartz crystal will do likewise in less than 1 s. Consequently, over the period (on the order of minutes and greater) that seems likely for the formation and evolution of hourglasses (see below), it can safely be assumed that the temperature within the inclusion is buffered by that in the surrounding magma. If the surrounding magma is gas saturated and decompressing, two competing processes will occur: (1) the quartz will tend to grow and enclose the inclusion because decompression causes H_2O to exsolve thereby increasing the liquidus temperature of the ambient magma; (2) a bubble in an hourglass will expand with decompression and expel liquid through the neck thus tending to keep the neck open. Because the neck constricts the flow, the pressure within the inclusion will be greater than the ambient magma pressure outside the quartz. Consequently, the concentration of H_2O in the expelling melt will be greater than that in the magma outside where quartz is crystallizing. (Loss of H_2O from an hourglass by means of rapid diffusion of H is limited by the small dissociation constant for H_2O and by the inclusion's negligible redox capacity in comparison with the available H_2O [total oxidation of 0.5 wt% of FeO to Fe_2O_3 would consume less than 0.07 wt% of H_2O].) For a given external decompressive supercooling necessary for continued crystallization of quartz, each hourglass may approach a steady state condition whereby further narrowing of the neck would result in a sufficiently large pressure (and activity of H_2O) within the hourglass that the melt in the neck of the hourglass would not precipitate quartz. In this way, the neck would not grow shut. Consequently, hourglasses have more gas than enclosed inclusions. According to this interpretation, two conditions must be met in order for hourglasses to form: (1) the magma parcel must be supercooled by effervescent decompression, and (2) there must be a gas bubble in the forming hourglass. If this idea is upheld, we may infer from hourglasses that the magma containing them was (1) gas saturated, and (2) decompressing.

Hourglass formation by the above process underscores the obstacles to the entrapment of bubbles of gas in crystals of quartz growing in gas-saturated decompressing magma. If a bubble-bearing reentrant or hourglass begins to grow shut, pressure in the bubble causes melt relatively rich in H_2O to extrude through the neck and keep it open. If there is no bubble, the reentrant just grows shut and forms an inclusion. If there is no gas in the system, there are no bubbles to be trapped and inclusions lack primary bubbles. If there is gas in the system, then there are two possibilities: (1) the forming inclusion has no bubble and grows shut, and (2) the forming inclusion has a bubble, and because of this, it cannot grow shut. Instead, it forms an hourglass. In sum, physical factors lead to two preferred outcomes: (1) an enclosed inclusion with no bubble and (2) an hourglass with a bubble.

Assumptions and applications to the Bishop hourglass inclusions

To apply the physical model outlined above and presented in Appendix 1 to observational data, I make the following necessary (1–4) and convenient (5–12) assumptions:

1. The hourglass neck remained unchanged during melt loss.
2. There is a primary gas bubble, or there is a negligible delay in the nucleation of the first gas bubble.
3. Decompression was simultaneous for all hourglasses in a single pumice clast.
4. Decompression was equal for all hourglasses in a single pumice clast.

(As I discuss later, if sufficient data are available, it is possible to test assumptions 3 and 4 and show that they are not valid for all hourglasses in a single pumice clast.)

5. Decompression is isothermal.
6. Enclosed melt inclusions and related hourglasses had the same initial, bulk (gas + melt) volatile contents.
7. Equilibrium is maintained between gas bubbles and melt.
8. Only melt (no gas) is lost from the hourglass.
9. Any primary bubble was volumetrically negligible.
10. Decompression was instantaneous.
11. Any yield strength of the melt is negligible compared to the 1000 bar/mm pressure gradients in the hourglass necks.
12. The flow regime in the necks was laminar.

All but four of the assumptions seem reasonable. Space does not permit presentation of all of the justifications. Below, I discuss briefly the four assumptions that I find to be problematical.

Assumption 1. Except for possible stagnant periods (no pressure gradient in the neck) when diffusion might be important, the amount of melt that has been lost through the neck is the amount of melt that could deposit or erode quartz in the neck. I expect change in SiO_2 to be caused by and proportional to a drop in H_2O content of the hourglass melt (corresponding to the gas content—32 vol% for hourglass 20). Associating the maximum range in SiO_2 with the near maximum amount of gas for hourglass 20 yields my estimate of $0.03/0.3 = 0.1$ for the change in mass fraction of SiO_2 in melt per volume fraction of gas in the hourglass. Inclusions with narrow necks (large hourglass numbers) are most affected. Applying this reasoning to inclusion 45, with one of the largest hourglass numbers, yields the result that the diameter of the neck decreased from 2.5 to 1.5 μm as a result of quartz deposited from the escaping decompressed melt. The corresponding effect on the hourglass number is approximately a factor of eight. This is an overestimate because the early evolution of the hourglass is dominated by CO_2-rich gas that has little effect on liquidus relations and because temperature is assumed constant, but this value may rise with rapid release of latent heat of crystallization.

Assumption 4. External (decompressed) pressures possibly differed for the various hourglasses. This possibility is suggested by the variable vesicularity within clasts of pumice and in glass adhering to phenocrysts. Shear of magma approaching the vent would be expected to bring together material from different initial depths (see Spera, 1984; Spera et al., 1986; Blake and Ivey, 1986). However, this would only be important in the case where the hourglasses did most of their emptying at pressures within the body of magma below the eruptive conduits. The results and discussion below reveal that this is likely only for hourglasses with less than approximately 3 vol% of gas. Wilson et al. (1980) point out the likelihood of recycling of large clasts in the conduit near the depths of magma disruption. Recycling would allow recombination of magma bits with varied decompression histories.

Assumption 8. It is at least conceivable that one or more tiny bubbles of gas could be lost with the melt through the neck. This will not make a big difference because the lost gas, like lost melt, would be compensated by new gas volume within the hourglass. In addition, the relatively low density of the gas limits the amount of volatile lost, but loss of gas could remove significant CO_2. Eventually analyses of hourglass volatiles (in glass and restored gas bubbles) can be compared with those of enclosed inclusions. If there has been significant loss of gas, the bulk CO_2 content of the hourglass will be low.

Assumption 9. The assumption that the amount of gas present before decompression was negligible is inconsistent with the proposed origin of the hourglasses. However, for hourglasses with more than a few vol% of gas, it probably is a satisfactory approximation. The primary bubble inferred for hourglass 20 is only 2.5 vol% at 1400 bars and would be less at greater pressures. We may expect problems for hourglasses with small amounts of gas. This means that the quenching pressure is constrained with greater confidence than is the duration of decompression, since the duration depends mostly on hourglasses that are poor in gas. For these hourglasses, both the presence of an initial bubble and the β-α inversion pose significant problems.

Estimation of melt viscosity

In calculating the curves on Figure 6, I approximated the melt viscosity with an exponential function of temperature and H_2O dissolved in the melt (Appendix 1, Eq. 22, approximated from Shaw, 1972). I assumed constant temperatures equal to those of preeruptive intratelluric crystallization (790 °C for Mono magma and 725 °C for plinian magma) documented by Hildreth (1979). Recalibrations of the Fe-Ti oxide geothermometer (see Stormer, 1983; Andersen and Lindsley, 1988; Tacker, personal communication) shift temperatures upward by approximately 35 °C. These changes, if adopted, would decrease the times calculated for emptying the hourglasses by approximately a factor of 3.

Plinian ash-fall hourglass inclusions

By comparing observed fractions and dimensions (hourglass numbers) of hourglasses with appropriate computed isochrons, it is possible to estimate both the (minimum) duration of time and the quenching (or external) pressure. Although subjective, this procedure yields a useful range of conditions appropriate for various plausible initial conditions.

Hourglasses in the plinian pumices are irregular and their hourglass numbers have large uncertainties. Nevertheless, a plot of gas fraction vs. hourglass number (Fig. 6A) reveals the expected negative correlation for seven out of nine hourglasses. Six of the seven are from the same clast of pumice, B104-F. Hourglass 58, also from B104-F, is unusual in that it terminates on a conchoidal fracture and is carrot shaped. The spread of points on Figure 6 suggests a two-minute duration of decompression. Time is so short that nonuniform cooling of pumice blocks larger than 10 cm in diameter might be expected to cause detectable variation in evolution times. A quenching pressure as small as approximately 400 bars is likely. The implied speed of ascent from 1800 to 400 bars is approximately 40 m/s. If a constant speed of ascent of 30 m/s (10 bars/s) is assumed, then the total plinian evolution time is increased to 3 min.

The Mono ash-flow lobe hourglass inclusions

Mono hourglasses (Fig. 6B, 6C) range over 5 orders of magnitude from 300 to 2.5×10^7 and may be put into three groups: (1) five hourglasses with very large hourglass numbers and uniformly small gas fractions (nos. 40, 45, 75, 84, and 116); (2) eight hourglasses forming the lower bound in terms of gas fraction [nos. 11, 38, 50, 55, 65 (off scale at HGN = 300 and gas fraction = 0.1), 70, 85, 110]; and (3) the remaining seven hourglasses.

The Mono hourglasses cannot be explained by any single isochron (Fig. 6) representing instantaneous decompression. In view of their near-rim location, Mono hourglasses are probably best interpreted as evolving from melts like the low-CO_2 inclusions (Fig. 6C), since both probably formed late in decompressing magma. However, comparison with Figure 6B (for the high CO_2 case) shows that this choice is not crucial. My interpretation is as follows. (1) The broad negative relation between gas fraction and hourglass number for the first two groups indicates that the idea of emptying through the neck as a result of decompression is valid for the Mono as well as plinian hourglasses. (2) Hourglass 65 (off scale on Fig. 6B, 6C) has such a small hourglass number (300) that it would evolve in less than 5 min at 790 °C and 8 h at 635 °C. [Hourglass 23 (also off scale on Fig. 6B), although of problematical character, provides a similar result: 12 min at 790 °C.] Assuming similar cooling [reasonable for hourglasses in the large block (18A) because its depositional temperature was likely near or below 635 °C—see below], an hourglass with hourglass number of 3000 would evolve only 1 vol% gas while hourglass 65 evolved its 10 vol% gas. Hourglass 65 thus limits posteruptive gas evolution in most other Mono hourglasses to negligible amounts. This limit and the glass coatings on quartz at the ends of necks suggest that most hourglasses evolved mainly before extrusion and in melt-rich (thus gas-poor, high-pressure, and hot) environments. (3) The low gas fractions in the group 1 hourglasses with large hourglass numbers suggest a common decompression history in preference to an accidental coincidence of similar primary gas fractions. Because isochrons that fit group 1 hourglasses are too long for group 2 hourglasses, I consider these groups separately.

Group 1 hourglasses possibly reflect pressure equilibration within a partially decompressed environment. I assume that 0.5 vol% of gas was produced by shrinkage (suggested by analogy with shrinkage bubbles in associated inclusions). The remaining 2.0 vol% of gas corresponds to an internal pressure of approximately 1.1 kbar, assuming an initial high CO_2 melt composition appropriate for the high CO_2 Mono lobe inclusions (Anderson et al., 1989a; Skirius et al., 1990; see Fig. 5). The 1.1 kbar value is in the range of gas saturation pressures for low CO_2 inclusions from the same clasts (Skirius et al., 1990) and less than most plinian inclusions. Thus, it is self-consistent to suggest that, during or after and as a consequence of eruption of plinian magma, the Mono magma decompressed to 1.1 kbar from an initial pressure of 2.4 kbar. Crystallization caused by the supersaturation attending effervescent decompression plausibly gave rise to a group of inclusions and hourglasses that formed at approximately 1.1 kbar. Computations show that, if hourglass 45 (Fig. 6C) evolved 2.0 vol% gas as a result of external decompression from 2.4 to 1.1 kbar, the time required is at least approximately 5×10^5 s (roughly a week).

Group 2 hourglasses bounding the lower limit of the gas fraction fit roughly an intermediate isochron marked by a quenching pressure of approximately 0.7 kbar and approximately 10^4 s (a few hours). The isochrons are more negatively sloped than the data, however, suggesting an acceleration of decompression with time, as might be expected for expanding magma rising into a uniform or narrowing conduit. If these hourglasses started out with 2% gas, like the low-gas hourglasses, then the time for their ascent and decompression would be only approximately 1000 s (15 min). The amount of gas that the five hourglasses with huge hourglass numbers would have gained during their last 15 min at 790 °C is negligible. The implied rate of ascent from 1.1 kbar to the quenching pressure of 0.7 kbar is about 1 m/s.

The remaining Mono hourglasses (nos. 20, 26, 74, 82, 83, 97, and 111) have anomalously large gas fractions (Fig. 6B). Of these hourglasses, 82, 97, and 111 are perhaps within the large uncertainties of the group 2 hourglasses. Either the anomalous hourglasses had initially large fractions of gas or they decompressed to considerably lower pressures than the main group before being coextruded or both. The textural and compositional data for hourglass 20 indicate preeruptive decompression to an external pressure of 0.4 kbar or less. Because its hourglass number is in the same range as the low-gas hourglasses, but it evolved much more gas, it must have been in a decompressed environment for a longer time (about 2 weeks at least). Similar interpretations may be valid for the other anomalous hourglasses.

It is noteworthy that the time (weeks) needed to partially empty hourglass 20 is similar to the time needed to

equilibrate the gas-poor hourglasses at 1100 bars. Both of these are, however, minimal times. Because hourglass 20 has a plinian-like K_2O content, I suggest that its estimated duration of decompression reflects an interval of time separating eruption of the plinian magma from the Mono magma. Although an eruption duration of two weeks is significantly less than suggested by the work of Snow and Yund (1988), Hildreth (1979, personal communication, 1990) considers that the lack of significant erosional breaks is best explained in terms of a continuous eruption of short duration. Further studies of hourglasses from other parts of the Bishop Tuff are needed to check on the relations between hourglass evolution and eruption history.

Hourglasses, eruption dynamics, and quenching history

I have argued above, on the basis of observed textures, that both the plinian and Mono hourglasses evolved largely before deposition and postdepositional cooling. This restricts postdepositional cooling to low temperatures (and high melt viscosities) or short times or both. Plinian pumice will be cooled below approximately 400 °C by entrained air probably within 10 s of magma disruption (Wilson et al., 1980; Woods, 1988). Models of ash-flow producing eruptions suggest that a Bishop-like rhyolitic magma with approximately 5 wt% H_2O would (1) cool by approximately 30 °C in less than 10 s due to gas expansion between the depth of magma disruption and the vent (Wilson et al., 1980); (2) entrain enough air in a collapsing eruption column to cause cooling of another 80 °C in approximately 20 s (Sparks et al., 1978; Woods, 1988); and (3) cool by less than approximately 45 °C during approximately 200 s of ash-flow transport (Boyd, 1961; Sparks et al., 1978). Although the above figures depend on many unknown parameters such as eruption rate, vent size and shape, preeruption gas content, etc. and can only be regarded as crude guides, it is evident that, compared with the times for evolution of plinian as well as Mono hourglasses, the predepositional cooling is likely to be fast. The amount of such cooling, however, need not be large for ash flows.

If predepositional cooling was small (<150 °C), then postdepositional evolution of hourglasses can be significant. Near the sample site for Mono ash-flow sample LV81-18A the ash flow is densely welded and vitrophyric indicating that some Mono ash-flow material reached the sampling locality while hot enough to weld (>625 °C—Smith, 1960). A temperature as high as 635 °C is consistent with the coolings enumerated above if the intratelluric crystallization temperature was 790 °C (Hildreth, 1977, 1979). The exact cooling environment of the Mono sample is unknown, but the relations at the outcrop suggest that most samples would have cooled at elevations less than approximately 5 m from cold ground. According to conductive theory, the clast might have remained warmer than 600 °C for approximately 1 yr. Most hourglasses would evolve a significant amount of gas at 635 °C in a year if they contained 4 wt% of H_2O and 100 ppm of CO_2 dissolved in the melt. Based on hourglass LV81-18A-65 (HGN = 300), this did not occur, possibly because the nonwelded Mono clast was deposited at or below approximately 600 °C (significantly below that temperature considered necessary for welding).

The magma ascent rate of approximately 40 m/s implied by plinian hourglasses is consistent with modeled rates of ascent of 2–100 m/s below the level of magma disruption (Wilson et al., 1980). The magma ascent rate of 1 m/s implied by the eight Mono hourglasses with 3–10 vol% of gas is consistent with a maximum ascent rate of approximately 1 m/s for magmatic foam feeding a collapsing (ash-flow producing) fountain [the maximum vent (1 bar) velocity of a collapsing fountain of rhyolitic magma with 5 wt% H_2O is approximately 70 m/s (Woods, 1988)]. The 700 bar quenching pressure of the Mono hourglasses, although notably greater than predicted magma disruption pressures (less than approximately 400 bars), seems not surprising in view of long vesicles in Mono pumice that suggest qualitatively high pressure quenching deep in a constricted conduit before vesicles could expand and become equant. Possibly magma disruption is aided by decompression transients associated with tensional cracking of the conduit.

A weeks-long eruption duration for the 600 km^3 Bishop Tuff is consistent with theoretically predicted mass-eruption rates (Wilson et al., 1980; Woods, 1988) for big rhyolitic eruptions. The implication that significant crystal growth (entrapment of low-pressure melt inclusions and evolution of gas-poor hourglasses with hourglass numbers $>10^6$) occurred during the eruption may be problematical. However, it is noteworthy that latent heat released by rapid crystallization in response to effervescent decompression would heat the magma and could help account for the observed increase in temperature.

Some key assumptions in the above logic are that the gas bubbles suffered negligible delay in nucleating, that the gas bubbles had time to equilibrate and grow, and that the preeruptive concentration of H_2O in the hourglass melt was roughly the same as that in enclosed inclusions. These assumptions can be argued and tested. In the meantime, future work should make use of geological tests by studying hourglasses from separate clasts of stratigraphically equivalent pumice at various distances from the cold ground.

Conclusions

Hourglass inclusions probably form in gas-saturated, decompressing magma as growing phenocrysts surround reentrants of melt that contain a tiny bubble of gas. Decompression causes melt to be lost through a narrow neck that is kept open because of the higher concentration of H_2O within the hourglass melt than in the surrounding decompressed magma. As melt is lost, an equal volume of gas forms within the hourglass. Consequently, the amount of gas in the hourglass increases. A quantitative model of the emptying process can be used to constrain

both the duration and extent of decompression from textural data. In addition, it is possible to estimate the mass and size of initial (high-pressure) gas bubbles in magma by comparing the bulk volatile contents of hourglasses and coeval inclusions.

The concepts have been applied to hourglasses from parts of the Bishop Tuff with the following results:

Plinian magma ascended rapidly (~40 m/s) as expected.

Some Mono magma first decompressed from approximately 2.4 kbar to approximately 1.1 kbar over a period of approximately a week. Final decompression to approximately 700 bars took approximately 15 min, implying a final ascent at 1 m/s. One (perhaps several) hourglass was repressurized after being at 400 bars or less for a week or two, at least. The week-long duration may relate to the interval of time between the eruption of the plinian pumice fall and the Mono ash-flow lobe. The pressure of eruptive quenching (disruption of foam into spray?) was approximately 700 bars.

Inclusion LV81-18A-20 (derived from plinian-like magma but extruded in the Mono ash-flow lobe) probably had a primary gas bubble 50 μm in diameter at a pressure of 1400 bars.

Hourglass inclusions preserve a record of eruptive phenomena on time scales ranging from minutes to weeks, at least. They can provide a temporal view of the filling and evacuation of near-surface magma bodies that is otherwise accessible only from theory. Hourglasses should be used together with enclosed inclusions to investigate durations of eruptions and eruptive interludes, to investigate rates of magma ascent, and to constrain the storage depth of preeruptive magma. This may lead to a better understanding of eruption mechanisms and preeruptive phenomena.

Acknowledgments

I especially thank Christine Skirius and Fangqiong Lu, two graduate students at Chicago, for their helpful questions and discussions. In addition, I am indebted to Skirius for obtaining and assessing the data of Table 2. I thank Wes Hildreth for some samples and Tim Druitt, Fred Nagle, and Stan Williams for other samples and for facts and ideas about field and textural relations. Discussions with Wes Hildreth, Roy Bailey, Charlie Bacon, Bill Rose, and Gerhard Wörner were helpful. John Wolff drew my attention to the important work by Donaldson and Henderson. I am grateful to Ed Roedder, Bill Nash, and Wes Hildreth for reviewing the manuscript. I owe a great debt to Sally Newman and Ed Stolper for advice and help. Of course, I alone am responsible for any errors. Parts of this work were supported by NSF grants 85-20934 and 89-04070 and DOE contract 10763.

References cited

Andersen, D.J., and Lindsley, D.H. (1988) Internally consistent solution models for Fe-Mg-Mn-Ti oxides: Fe-Ti oxides. American Mineralogist, 73, 714–726.

Anderson, A.T., Jr., Newman, S., Williams, S.N., Druitt, T.H., Skirius, C., and Stolper, E. (1989a) H_2O, CO_2, Cl and gas in plinian and ash-flow Bishop rhyolite. Geology, 17, 221–225.

Anderson, A.T., Jr., Skirius, C.M., Lu, F., and Davis, A.M. (1989b) Preeruption gas content of Bishop plinian rhyolitic magma. Geological Society of America Abstracts with Programs, 21, no. 6, A270.

Bacon, C.R. (1989) Crystallization of accessory phases in magmas by local saturation adjacent to phenocryst. Geochimica et Cosmochimica Acta, 53, 1055–1066.

Bailey, R.A., Dalrymple, G.B., and Lanphere, M.A. (1976) Volcanism, structure, and geochronology of Long Valley caldera, Mono County, California. Journal of Geophysical Research, 81, 725–744.

Beddoe-Stephens, B., Aspden, J.A., and Shepherd, T.J. (1983) Glass inclusions and melt compositions of the Toba tuffs, northern Sumatra. Contributions to Mineralogy and Petrology, 83, 278–287.

Blake, S., and Ivey, G.N. (1986) Density and viscosity gradients in zoned magma chambers, and their influence on withdrawal dynamics. Journal of Volcanology and Geothermal Research, 30, 201–230.

Blank, J.G., Stolper, E.M., Sheng, J., and Epstein, S. (1989) The solubility of CO_2 in rhyolitic melt at pressures to 1500 bars. Geological Society of America Abstracts with Programs, 21, A157.

Boyd, F.R. (1961) Welded tuffs and flows in the rhyolite plateau of Yellowstone Park, Wyoming. Geological Society of America Bulletin, 72, 387–426.

Burnham, C.W. (1979) The importance of volatile constituents. In H.S. Yoder, Jr., Ed., The evolution of the igneous rocks. Fiftieth anniversary perspectives, p. 439–482. Princeton University Press, Princeton, New Jersey.

Donaldson, C.H., and Henderson, C.M.B. (1988) A new interpretation of round embayments in quartz crystals. Mineralogical Magazine, 52, 27–33.

Flowers, G. C. (1979) Correction of Holloway's (1977) adaptation of the modified Redlich-Kwong equation of state for calculation of the fugacities of molecular species in supercritical fluids of geological interest. Contributions to Mineralogy and Petrology, 69, 315–318.

Ghiorso, M.S., Carmichael, I.S.E., and Moret, L.K. (1979) Inverted high-temperature quartz; unit cell parameters and properties of the alpha-beta inversion. Contributions to Mineralogy and Petrology, 68, 307–323.

Gilbert, C.M. (1938) Welded tuff in eastern California. Geological Society of American Bulletin, 49, 1829–1862.

Hildreth, E.W. (1977) The magma chamber of the Bishop Tuff: Gradients in temperature, pressure and composition, 328 p. Ph.D. thesis, University of California, Berkeley, Berkeley, California.

——— (1979) The Bishop Tuff: Evidence for the origin of compositional zonation in silicic magma chambers. Geological Society of America Special Paper, 180, 43–75.

Holloway, J.R. (1977) Fugacity and activity in molecular species in supercritical fluids. In D. Fraser, Ed., Thermodynamics in geology, p. 161–181. Reidel, Dordrecht, The Netherlands.

Kozlowski, A. (1981) Melt inclusions in pyroclastic quartz from the Carboniferous deposits of the Holy Cross Mts., and the problem of magmatic corrosion. Acta Geologica Polonica, 31, 273–284.

Lu, F., Davis, A.M., Skirius, C.M., and Anderson, A.T., Jr. (1989) Significance of uranium variations in rhyolitic melt inclusions from the Bishop plinian and early ash-flow deposits. Geological Society of America Abstract with Programs, 21, no. 6, A271.

Lu, F., Anderson, A.T., Jr., and Davis, A.M. (1990) Implications of glass inclusions for the origins of high silica rhyolite and compositional zonation of the Bishop Tuff, California. Eos, 71, 651.

Newman, S., Epstein, S., and Stolper, E. (1988) Water, carbon dioxide, and hydrogen isotopes in glasses from the ca. 1340 A.D. eruption of the Mono Craters, California: Constraints on degassing phenomena and initial volatile content. Journal of Volcanology and Geothermal Research, 35, 75–96.

Roedder, E. (1979) Origin and significance of magmatic inclusions. Bulletin Minéralogique, 102, 487–510.

Shaw, H.R. (1972) Viscosities of magmatic silicate liquids: An empirical method of prediction. American Journal of Science, 272, 870–893.

Sheridan, M.F. (1965) The mineralogy and petrology of the Bishop Tuff, 165 p. Ph.D. thesis, Stanford University, Palo Alto, California.

——— (1967) Double cooling unit nature of the Bishop tuff in Owens River Gorge, California (abs.). Geological Society of America, Special Paper, 115, 351.

Silver, L.A., Ihinger, P.D., and Stolper, E. (1990) The influence of bulk composition on the speciation of water in silicate glasses. Contributions to Mineralogy and Petrology, 104, 142–162.

Skirius, C.M. (1989) Pre-eruptive H_2O and CO_2 in Plinian and early ash flow magma of the Bishop Tuff (abs.). IAVCEI Abstracts, New Mexico Institute of Mines and Mineral Resources Bulletin, 131, 245.

Skirius, C.M., Peterson, J.W., and Anderson, A.T., Jr. (1990) Homogenizing rhyolitic glass inclusions from the Bishop Tuff. American Mineralogist, 1381–1398.

Smith, R.L. (1960) Zones and zonal variations in welded ash-flows. U.S. Geological Survey Professional Paper, 345-f.

Snow, E., and Yund, R.A. (1988) Origin of cryptoperthites in the Bishop tuff and their bearing on its thermal history. Journal of Geophysical Research, 93, 8975–8984.

Sparks, R.S.J., and Brazier, S. (1982) New evidence for degassing processes during explosive eruptions. Nature, 295, 218–220.

Sparks, R.S.J., Wilson, L., and Hulme, G. (1978) Theoretical modeling of the generation, movement and emplacement of pyroclastic flows by column collapse. Journal of Geophysical Research, 83, 1727–1739.

Spera, R.J. (1984) Some numerical experiments on the withdrawal of magma from crustal reservoirs. Journal of Geophysical Research, 89, 8222–8236.

Spera, R.J., Yuen, D.A., Greer, J.C., and Sewell, G. (1986) Dynamics of withdrawal from stratified magma chambers. Geology, 14, 723–726.

Stormer, J.C. (1983) The effects of recalculation on estimates of temperature and oxygen fugacity from analyses of multi-component iron-titanium oxides. American Mineralogist, 68, 586–594.

Tait, S.R., and Jaupart, C. (1990) Selective preservation of melt inclusions in crystals. Eos, 71, 650.

Watson, E.B., Sneeringer, M.A., and Ross, A. (1982) Diffusion of dissolved carbonate in magmas: Experimental results and applications. Earth and Planetary Science Letters, 61, 346–358.

Whitham, A.G., and Sparks, R.S.J. (1986) Pumice. Bulletin of Volcanology, 48, 209–223.

Wilson, L., Sparks, R.S.J., and Walker, G.P.L. (1980) Explosive volcanic eruptions IV. The control of magma properties and conduit geometry on eruption column behavior. Geophysical Journal of the Royal Astronomical Society, 63, 117–148.

Woods, A.W. (1988) The fluid dynamics and thermodynamics of eruption columns. Bulletin of Volcanology, 50, 169–193.

Manuscript received April 4, 1990
Manuscript accepted January 11, 1991